

Spin- and valley-dependent magneto-optical properties of MoS₂

Félix Rose,^{1,2} M. O. Goerbig,¹ and Frédéric Piéchon¹

¹*Laboratoire de Physique des Solides, CNRS UMR 8502, Université Paris-Sud, F-91405 Orsay Cedex, France*

²*Physics Department, École Polytechnique, 91128 Palaiseau, France*

(Received 16 July 2013; published 30 September 2013)

We investigate the behavior of low-energy electrons in two-dimensional molybdenum disulfide when submitted to an external magnetic field. Highly degenerate Landau levels form in the material, between which light-induced excitations are possible. The dependence of excitations on light polarization and energy is explicitly determined, and it is shown that it is possible to induce valley and spin polarization, i.e., to excite electrons of selected valley and spin. Whereas the effective low-energy model in terms of massive Dirac fermions yields dipole-type selection rules, higher-order band corrections allow for the observation of additional transitions. Furthermore, inter-Landau-level transitions involving the $n = 0$ levels provide a reliable method for an experimental measurement of the gap and the spin-orbit gap of molybdenum disulfide.

DOI: [10.1103/PhysRevB.88.125438](https://doi.org/10.1103/PhysRevB.88.125438)

PACS number(s): 78.20.-e, 75.70.Tj, 78.67.-n

I. INTRODUCTION

Molybdenum disulfide (MoS₂), in its two-dimensional (2D) form, has recently been isolated via the exfoliation technique, similarly to graphene and 2D boron nitride.¹ In contrast to bulk or few-layer MoS₂, which is an indirect-gap semiconductor, recent experiments have shown that 2D MoS₂ is a semiconductor with a direct gap on the order of 1.66 eV,^{2,3} in agreement with *ab initio* and tight-binding calculations.^{4–11} The direct gap is situated at the corners \mathbf{K} and $\mathbf{K}' = -\mathbf{K}$ of the hexagon-shaped first Brillouin zone. In the vicinity of these points (valleys) and at low energy, the electronic properties can be modeled by massive Dirac fermions with a moderate spin-orbit coupling.^{5,12} This opens the fascinating possibility to study the particular topological properties of pseudorelativistic fermions in a condensed-matter system other than graphene where the low-energy electronic properties are governed by massless Dirac fermions.¹³ Recent experiments have indeed shown^{14,15} that circularly polarized light allows one to address electrons in a single valley, in agreement with previous analytical¹² and numerical *ab initio*¹⁶ calculations, such that MoS₂ might be a promising candidate for valleytronics devices.

One of the most salient features of 2D Dirac fermions in condensed-matter systems is certainly their topological property in the form of a singularity in the wave function at the (massive) Dirac point that gives rise to a nonzero Berry curvature.^{17,18} A prominent consequence is an anomaly in the $n = 0$ Landau level in the presence of a magnetic field, which in contrast to all other levels is bound either to the top of the valence or the bottom of the conduction band.

In the present paper, we study the magneto-optical properties of 2D MoS₂, which arise precisely due to the presence of massive Dirac fermions in the vicinity of the \mathbf{K} points. Whereas the $n = 0$ Landau level at the \mathbf{K} point is situated at the top of the valence band, that at the \mathbf{K}' point is bound to the bottom of the conduction band. As a consequence, circularly polarized light allows one to excite electrons in a single valley if the inter-Landau-level transition involves the $n = 0$ level. This transition provides a direct measure of the mass gap and the spin-orbit coupling in MoS₂. Very similar results have recently been obtained by Tabert and Nicol, who investigated the magneto-optical properties of silicene and similar 2D materials

that may also be described in terms of massive Dirac fermions at low energy.^{19,20} Whereas massive Dirac fermions respect the dipole selection rules $n \rightarrow n \pm 1$ (regardless of the band), we show furthermore that higher-order band corrections such as trigonal warping give rise to additional allowed transitions, such as the interband transitions $n \rightarrow n$ or $n \rightarrow n \pm 2$ and $n \rightarrow n \pm 4$.

The remaining parts of the paper are organized as follows. In Sec. II, we build up the model Hamiltonian, which is discussed in the absence and the presence of a magnetic field, the latter giving rise to the Landau-level spectrum. The magneto-optical excitations within the model of massive Dirac fermions with spin-orbit coupling are investigated in Sec. III, where the selection rules for MoS₂ are presented. Section IV is devoted to a study of band corrections, their influence on the Landau-level spectrum, and optical transitions beyond the dipole-allowed ones.

II. GENERAL OVERVIEW

In this section, we characterize the low-energy behavior of electrons in MoS₂ in both the absence and the presence of a transverse magnetic field. We begin by introducing the Dirac Hamiltonian and the spin-orbit coupling before considering the effect of a magnetic field.

A. Low-energy Hamiltonian

The electronic behavior of MoS₂ has been studied both in the framework of *ab initio* and tight-binding calculations.^{4,5,8,10,12} The material has one molybdenum and two sulfur atoms per unit cell (see Fig. 1), and in total 11 orbitals thus need to be considered: three p orbitals for each of the sulfur and five d orbitals from the molybdenum atoms. In contrast to bulk or few-layer MoS₂, which is an indirect-gap semiconductor,^{7,9,11} a single layer of MoS₂ has a direct gap of roughly 1.66 eV at the \mathbf{K} and $\mathbf{K}' = -\mathbf{K}$ points situated at the corners of the hexagonal first Brillouin zone.¹¹ In spite of the complexity of the band structure, the low-energy electronic properties of MoS₂, in the vicinity of the two valleys \mathbf{K} and \mathbf{K}' , may be understood within a simplified model that only takes into account three molybdenum orbitals: $|d_{3z^2-z^2}\rangle$,

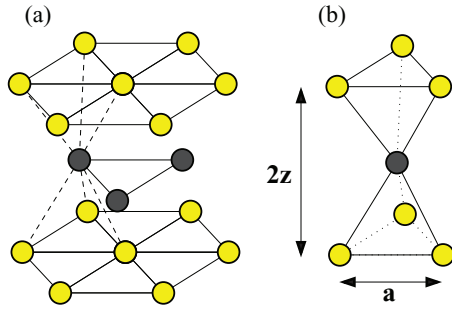


FIG. 1. (Color online) Crystal structure of 2D MoS₂. (a) Perspective view of the honeycomb lattice. (b) The unit cell. Each of the two sulfur atoms of the *A* sublattice (purple) is separated by a length¹¹ $z \approx 1.572 \text{ \AA}$ from the *B* sublattice (red) plane. The characteristic lattice spacing¹¹ $\tilde{a} \approx 3.16 \text{ \AA}$ is defined as the distance between the two closest points in a sublattice.

which mostly forms the bottom of the conduction band, and a valley-dependent mix of $|d_{xy}\rangle$ and $|d_{x^2-y^2}\rangle$ for the top of the valence band,¹²

$$|\phi_c\rangle = |d_{3r^2-z^2}\rangle, \quad |\phi_v^\xi\rangle = \frac{1}{\sqrt{2}}(|d_{x^2-y^2}\rangle + i\xi |d_{xy}\rangle). \quad (1)$$

Here, $\xi = +$ denotes the valley \mathbf{K} and $\xi = -$ stands for \mathbf{K}' . If one represents the Hamiltonian in this basis and expands it around the points \mathbf{K} and \mathbf{K}' , the low-energy Hamiltonian of the system can be written as¹²

$$\hat{H}_0 = \hbar v_F (\xi q_x \sigma_x + q_y \sigma_y) + \Delta \sigma_z, \quad (2)$$

in which σ_x, σ_y , and σ_z are Pauli matrices, and \mathbf{q} is the reciprocal-lattice vector measured with respect to $\xi\mathbf{K}$ with $\tilde{a}|\mathbf{q}| \ll 1$ (\tilde{a} being the characteristic lattice spacing). Notice that the Fermi velocity $v_F \approx 85\,000 \text{ m/s}$ in MoS₂ is comparable to that of graphene.

B. Spin-orbit coupling

As mentioned above, MoS₂ is characterized by a strong intrinsic spin-orbit coupling (see Fig. 2). The spin-orbit

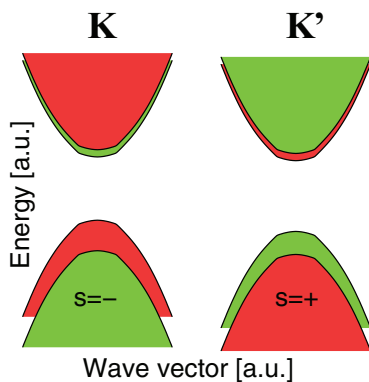


FIG. 2. (Color online) Sketch of the low-energy band structure of molybdenum disulfide in arbitrary units (a.u.). The band structure consists of two pairs of massive Dirac cones separated by spin-orbit coupling.

Hamiltonian, which needs to be added to \hat{H}_0 , is

$$\hat{H}_{so} = \xi \begin{pmatrix} \Delta_{so}^c & 0 \\ 0 & \Delta_{so}^v \end{pmatrix} \otimes s_z, \quad (3)$$

in which s_z is the Pauli matrix for spin (of eigenvalues ± 1) and $2\Delta_{so}^{c,v}$ is the spin-orbit gap in the conduction and valence band, respectively. *Ab initio* calculations indicate that $\Delta_{so}^v \approx 150 \text{ meV}$ while Δ_{so}^c is very small but finite ($\Delta_{so}^c \approx 3 \text{ meV}$). Thus, we note

$$\Delta_{so} = \Delta_{so}^v - \Delta_{so}^c \approx \Delta_{so}^v. \quad (4)$$

Obviously, as long as spin relaxation processes are not considered, the spin remains a good quantum number. It is noteworthy that $\Delta_{so}^{c,v} \ll \Delta$, and thus the low-energy physical properties in MoS₂ are largely controlled by the mass gap 2Δ . Therefore, in spite of the similarity with the model Hamiltonian used in the description of graphene with a spin-orbit gap²¹ or silicene,²² no quantum spin Hall effect is to be expected in MoS₂ because the latter would require $\Delta_{so}^{c,v} \gg \Delta$. Even if \hat{H}_{so} is different in each valley, it is locally constant around $\xi\mathbf{K}$ and therefore does not complicate the analysis of the orbital (wave-vector-dependent) electronic properties, such as the calculation of the Landau levels (see Sec. II C). Thus, the system is equivalent to two spin-resolved Dirac Hamiltonians similar to \hat{H}_0 with a spin- and valley-dependent gap $2\Delta_{\xi s}$ as well as a constant energy term,

$$\hat{H}_{\xi,s} = \hat{H}_0(\Delta = \Delta_{\xi s}) + \frac{\Delta_{so}^c + \Delta_{so}^v}{2} \mathbb{1}_2, \quad (5)$$

$$\Delta_{\xi s} = \Delta - \frac{\xi s}{2} \Delta_{so}. \quad (6)$$

The term of constant energy $(\Delta_{so}^c + \Delta_{so}^v)\mathbb{1}_2/2$ plays no physical role and is omitted henceforth.

C. Landau levels

When 2D electrons are subjected to a transverse magnetic field $\mathbf{B} = \nabla \times \mathbf{A}$, Landau levels form and the energies within the valence and conduction bands get quantized. Indeed, making the Landau-Peierls substitution $\mathbf{q} \rightarrow \mathbf{q} + e\mathbf{A}/\hbar$ in the Hamiltonian shows that it is possible to write the wave functions of the Hamiltonian as $|\psi_{\mathbf{k}}\rangle = \phi(x) \exp(ik_y y)$, in which ϕ is an eigenvector of the effective Hamiltonian,

$$\hat{H}_{\mathbf{B}}^{\xi,s} = \hbar v_F \left[\xi q_x \sigma_x + \left(k_y + \frac{eB}{\hbar} x \right) \sigma_y \right] + \Delta_{\xi s} \sigma_z, \quad (7)$$

where we have used the Landau gauge $\mathbf{A} = (0, Bx, 0)$ for the vector potential. Because x and q_x do not commute, it is possible to rewrite the Hamiltonian using dimensionless operators $Q = l_B q_x$ and $X = x/l_B + \hbar k_y/eB$ such that $[X, Q] = i$. Here, $l_B = \sqrt{\hbar/eB}$ is the magnetic length,

$$\hat{H}_{\mathbf{B}}^{\xi,s} = \frac{\hbar v_F}{l_B} (\xi Q \sigma_x + X \sigma_y) + \Delta_{\xi s} \sigma_z. \quad (8)$$

With the help of the ladder operators $a = (X + iQ)/\sqrt{2}$ and $a^\dagger = (X - iQ)/\sqrt{2}$, we may rewrite the Hamiltonian in both

valleys,

$$\hat{H}_{\mathbf{B}}^{\xi=+,s} = \begin{pmatrix} \Delta_s & -i\varepsilon a \\ i\varepsilon a^\dagger & -\Delta_s \end{pmatrix}, \quad (9)$$

$$\hat{H}_{\mathbf{B}}^{\xi=-,s} = \begin{pmatrix} \Delta_{-s} & i\varepsilon a^\dagger \\ -i\varepsilon a & -\Delta_{-s} \end{pmatrix}, \quad (10)$$

in which $\varepsilon = \sqrt{2}\hbar v_F / l_B \approx 30.5 \sqrt{B(T)}$ meV.

Using the eigenvectors $|n\rangle$ of the number operator $n = a^\dagger a$, it is possible to find the eigenstates of the Hamiltonian in both valleys,

$$\psi_{\lambda n}^{\xi=+,s} = (\alpha_{\lambda n}^{+,s} |n-1\rangle, \beta_n |n\rangle) \quad \text{for } n \geq 1, \quad (11)$$

$$\psi_{-0}^{\xi=+,s} = (0, |0\rangle) \quad \text{for } n = 0, \quad (12)$$

$$\psi_{\lambda n}^{\xi=-,s} = (\alpha_{\lambda n}^{-,s} |n\rangle, \beta_n |n-1\rangle) \quad \text{for } n \geq 1, \quad (13)$$

$$\psi_{+0}^{\xi=-,s} = (|0\rangle, 0) \quad \text{for } n = 0, \quad (14)$$

where $\lambda = \pm 1$ designates the band. Here, the coefficients $\alpha_{\lambda n}^{\xi,s}$ and β_n are defined as

$$\alpha_{\lambda n}^{\xi,s} = \Delta_{\xi s} + \lambda \sqrt{\Delta_{\xi s}^2 + n\varepsilon^2}, \quad (15)$$

$$\beta_n = -i\sqrt{n\varepsilon}. \quad (16)$$

Counting possible values of k_y yields that the Landau-level degeneracy is $n_B = eB/h$ for each of the four spin-valley branches.

Notice that the norm of the vector $\psi_{\lambda n}^{\xi,s}$ is the same for both valleys and will be noted as $N_{\lambda n}^{\xi,s}$,

$$N_{\lambda n}^{\xi,s} = \sqrt{|\alpha_{\lambda n}^{\xi,s}|^2 + |\beta_n|^2} \quad \text{for } n \geq 1, \quad N_{\lambda 0}^{\xi,s} = 1. \quad (17)$$

The energy associated with the spinor $\psi_{\lambda n}^{\xi,s}$ is

$$\varepsilon_{\lambda n}^{\xi,s} = \lambda \sqrt{\Delta_{\xi s}^2 + n\varepsilon^2} \quad \text{for } n \geq 1. \quad (18)$$

In contrast to the $n \neq 0$ levels, which occur in pairs in each valley (one for each band), the $n = 0$ level needs to be treated separately. Indeed, one finds a single $n = 0$ level per valley. In the present case, as $\Delta_{\xi s}$ is always positive (since $\Delta_{\text{so}} \ll \Delta$), for both values of spin the $n = 0$ Landau levels in the \mathbf{K} valley are fixed at the top of the valence band ($\varepsilon_{n=0}^{+,s} = -\Delta_{+,s}$) whereas the two $n = 0$ levels in the \mathbf{K}' valley are located at the bottom of the conduction band ($\varepsilon_{n=0}^{-,s} = \Delta_{-,s}$) (see Fig. 3). This is a direct consequence of the fact that electrons behave as massive Dirac fermions. The two valleys react differently to the magnetic field, and the particular behavior of the $n = 0$ Landau levels is due to the particular winding properties of the Berry phase, as may be understood in the framework of a semiclassical analysis.¹⁸

Notice finally that, if $2\Delta_{\text{so}} > \Delta$, Δ_+ is negative while Δ_- remains positive. Therefore, in both valleys, the $\psi_{\pm 0}^{\xi,s=+}$ states would be fixed to the bottom of the conduction band and the $\psi_{\pm 0}^{\xi,s=-}$ states are at the top of the valence band, which is a case discussed in the framework of silicene.^{19,20}

III. MAGNETO-OPTICAL EXCITATIONS

In the present section, we consider optical excitations between Landau levels of MoS₂ and establish selection rules

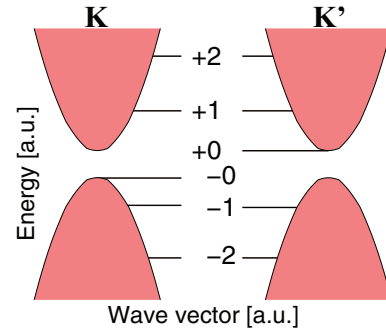


FIG. 3. (Color online) Representation of the Landau levels in the valleys \mathbf{K} and \mathbf{K}' when spin-orbit coupling is not taken into account, i.e., it is assumed that $\Delta_{\xi s} = \Delta$. In that peculiar case, the energy levels are spin-degenerate. For the sake of clarity, the figure is not to scale as the energy separating the closest Landau levels is much smaller than the gap.

depending on the circular polarization of the radiation. To that effect, we assume that the MoS₂ layer is exposed to circularly polarized light. We shall label \mathbf{k}_p the wave vector and $\hbar\omega$ the energy of the light field. \mathbf{k}_p is orthogonal to the plane of the material and much smaller than $1/\tilde{a}$, thus authorizing only vertical transitions. The polarization index is denoted as σ . For clockwise-polarized light $\sigma = +1$, otherwise $\sigma = -1$. We shall now determine interaction with light and the associated selection rules.

A. General theory

To take into account the coupling to the light field, one may again use the Landau-Peierls substitution with a modified total potential $\mathbf{A}_{\text{tot}} = \mathbf{A} + \mathbf{A}_{\text{rad}}(t)$, in which \mathbf{A} is the potential introduced earlier, and

$$\mathbf{A}_{\text{rad}}(t) = A \begin{pmatrix} \cos(\omega t) \\ \cos(\omega t - \sigma \frac{\pi}{2}) \\ 0 \end{pmatrix} \quad (19)$$

is the potential describing the light. The interaction between the light and electrons in the system is given by the Hamiltonian

$$\hat{H}_1(t) = \frac{e}{\hbar} \nabla_{\mathbf{k}} \hat{H}_{\mathbf{B}}^{\xi,s} \cdot \mathbf{A}(t)_{\text{rad}} = \hat{W}_{\xi\sigma} e^{-i\omega t} + \hat{W}_{\xi\sigma}^\dagger e^{i\omega t}, \quad (20)$$

which needs to be added to the Hamiltonian. Here,

$$\hat{W}_{\xi\sigma} = ev_F Ah_{\xi\sigma} \quad \text{with} \quad h_{\xi\sigma} = \frac{1}{2}(\xi\sigma_x + \sigma i\sigma_y), \quad (21)$$

where we have defined

$$h_{\xi s=+1} = \begin{pmatrix} 0 & 1 \\ 0 & 0 \end{pmatrix} \quad \text{and} \quad h_{\xi s=-1} = \begin{pmatrix} 0 & 0 \\ 1 & 0 \end{pmatrix}. \quad (22)$$

This may be treated as a time-dependent perturbation, and transitions between initial states $|i\rangle$ and final states $|f\rangle$ are possible only if their respective energies are related to ω by $E_f - E_i = \pm\hbar\omega$. The excitation term, which is what is interesting here, is proportional to $|\langle f | \hat{W}_{\xi s} | i \rangle|^2$ and thus to

TABLE I. Values of relative transition rates $\mathcal{P}_{\lambda_i n_i, \lambda_n f}^{\xi, s, \sigma}$ for every possible transition $|i\rangle \rightarrow |f\rangle$ are given as a function of the valley and light polarization. Here, n denotes a nonzero positive integer and the state labeled as $\psi_0^{\xi, s}$ is either $\psi_{-0}^{\xi=+1, s}$ in the \mathbf{K} valley or $\psi_{+0}^{\xi=-1, s}$ in the \mathbf{K}' valley.

Transitions	Valley and light polarization			
	$\xi = +1, \sigma = +1$	$\xi = +1, \sigma = -1$	$\xi = -1, \sigma = +1$	$\xi = -1, \sigma = -1$
$\psi_{-(n+1)}^{\xi, s} \rightarrow \psi_{\lambda n}^{\xi, s}$	0	$\left \frac{\alpha_{-(n+1)}^{+s} \beta_n}{N_{-(n+1)}^{+s} N_{\lambda n}^{+s}} \right ^2$	0	$\left \frac{\alpha_{\lambda n}^{-s} \beta_{n+1}}{N_{-(n+1)}^{-s} N_{\lambda n}^{-s}} \right ^2$
$\psi_{\lambda n}^{\xi, s} \rightarrow \psi_{n+1}^{\xi, s}$	$\left \frac{\alpha_{n+1}^{+s} \beta_n}{N_{\lambda n}^{+s} N_{n+1}^{+s}} \right ^2$	0	$\left \frac{\alpha_{\lambda n}^{-s} \beta_{n+1}}{N_{\lambda n}^{-s} N_{n+1}^{-s}} \right ^2$	0
$\psi_{-1}^{\xi, s} \rightarrow \psi_0^{\xi, s}$	0	$\left \frac{\alpha_{-1}^{+s}}{N_{-1}^{+s}} \right ^2$	0	$\left \frac{\beta_{-1}}{N_{-1}^{-s}} \right ^2$
$\psi_0^{\xi, s} \rightarrow \psi_{+1}^{\xi, s}$	$\left \frac{\alpha_{+1}^{+s}}{N_{+1}^{+s}} \right ^2$	0	$\left \frac{\beta_{+1}}{N_{+1}^{-s}} \right ^2$	0

$|\langle f | h_{\xi\sigma} | i \rangle|^2$. Hence, the transition rates are defined as

$$\mathcal{P}_{\lambda_i n_i, \lambda_n f}^{\xi, s, \sigma} = \left| \frac{(\psi_{\lambda_n f}^{\xi, s})^\dagger h_{\xi\sigma} \psi_{\lambda_i n_i}^{\xi, s}}{N_{\lambda_i n_i}^{\xi, s} N_{\lambda_n f}^{\xi, s}} \right|^2, \quad (23)$$

where we have explicitly taken into account the normalization (17) of the vectors. The number $\mathcal{P}_{\lambda_i n_i, \lambda_n f}^{\xi, s, \sigma}$ is comprised between 0 and 1, which indicates the relative amount of electrons that will be excited for a given transition. It is thus a measure of the strength of the associated absorption or emission peaks.

B. Selection rules

The above results can be used to determine which transitions are authorized for both polarizations in each valley. Considering the form of the vectors defined in Eqs. (11)–(14) and $h_{\pm 1}$, it is obvious that the only possible transitions are from states $\psi_{\lambda n_i}^{\xi, s}$ to $\psi_{\lambda n_f}^{\xi, s}$ such that n_i and n_f differ by exactly 1. Notice, however, that other transitions may occur if band corrections (such as trigonal warping) to the model are taken into account. We discuss these corrective terms in more detail in Sec. IV.

All possible transitions as well as the corresponding amplitudes are given in Table I and shown in Fig. 4. It appears that the authorized transitions are the same in both valleys, with the exception of transitions implying the $\psi_0^{\xi, s}$ states. Hence, those are the transitions interesting for valley polarization. Other possible transitions which are activated at different energies are not considered in the following sections.

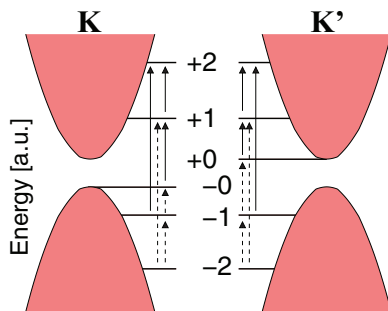


FIG. 4. (Color online) Possible optical transitions between Landau levels in the absence of spin-orbit coupling. Full arrows correspond to $\sigma = +1$ polarization whereas dashed arrows correspond to $\sigma = -1$ polarization.

If the Fermi level ε_F is comprised between $\varepsilon_{-1}^{\xi, s}$ and $\varepsilon_{+1}^{\xi, s}$, it is possible to polarize either valley using these transitions. To help characterize them, we define

$$\Delta_B^{\xi, s} = \varepsilon_{+1}^{\xi, s} - \varepsilon_{-0}^{\xi, s} \approx 2\Delta_{\xi, s}, \quad (24)$$

$$\delta_B^{\xi, s} = \varepsilon_{+1}^{\xi, s} - \varepsilon_{+0}^{\xi, s} \approx \frac{\varepsilon^2}{2\Delta_{\xi, s}}, \quad (25)$$

where we have used the fact that $\varepsilon \approx 30.5 \sqrt{B(T)}$ meV $\ll \Delta_{\xi, s}$. $\Delta_B^{\xi, s}$ is the energy associated with the $\psi_{-0}^{\xi=+1, s} \rightarrow \psi_{+1}^{\xi=+1, s}$ and $\psi_{-1}^{\xi=-1, s} \rightarrow \psi_{+0}^{\xi=-1, s}$ transitions, while $\delta_B^{\xi, s}$ is associated with the $\psi_{-1}^{\xi=+1, s} \rightarrow \psi_{-0}^{\xi=+1, s}$ and $\psi_{+0}^{\xi=-1} \rightarrow \psi_{+1}^{\xi=-1}$ transitions. The possible transitions involving the Landau level $n = 0$ are depicted in Fig. 5.

For the transitions discussed above, the relative amplitudes are readily calculated with the help of approximation (24),

$$\begin{aligned} \mathcal{P}_{-0, +1}^{\xi=+1, s, \sigma=+1} &= 1 - \frac{\varepsilon^2}{4\Delta_{\xi, s}^2}, & \mathcal{P}_{-1, -0}^{\xi=+1, s, \sigma=-1} &= \frac{\varepsilon^2}{2\Delta_{\xi, s}^2}, \\ \mathcal{P}_{-1, +0}^{\xi=-1, s, \sigma=+1} &= \frac{\varepsilon^2}{4\Delta_{\xi, s}^2}, & \mathcal{P}_{+0, +1}^{\xi=-1, s, \sigma=-1} &= 1 - \frac{\varepsilon^2}{2\Delta_{\xi, s}^2}. \end{aligned} \quad (26)$$

As $\varepsilon/\Delta_{\xi, s} \approx 10^{-2}$, the magnitudes of the transitions involving $\sigma = -\xi$ polarizations are expected to be much less intense than the $\sigma = \xi$ transitions.

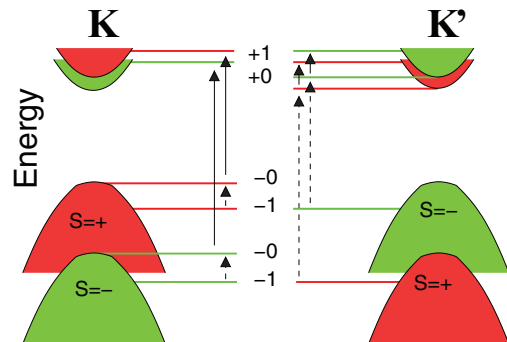


FIG. 5. (Color online) Possible optical transitions in undoped MoS₂ involving $\psi_{\lambda 0}^{\xi, s}$ states between Landau levels in the presence of spin-orbit coupling. The splitting is reversed between the two valleys. $s = +1$ corresponds to the red bands while $s = -1$ is represented by the green bands. The arrow signification remains the same as in Fig. 4. The figure takes into account the fact that $2\Delta \gg 2\Delta_{so}^v \gg \delta_B^{\xi, s}, \Delta_{so}^c$.

1. Transitions in undoped MoS₂

In the case of undoped MoS₂, that is, when the Fermi level is situated in the gap between the valence and the conduction band, the above analysis shows that it is possible to excite electrons in a single valley with use of circularly polarized light, similarly to the case of MoS₂ in the absence of a magnetic field.¹² In contrast to the latter case, the magnetic field has two major consequences: first, it defines well-separated energy levels that one may address in a resonant manner; second, the absorption and emission peaks are proportional to the density of states, which is strongly enhanced at resonance by the magnetic field because the density of states per Landau level is given by the flux density $n_B \propto B$. As depicted in Fig. 5, light with a polarization $\sigma = +$ is associated with the transition from -0 to $+1$ in the \mathbf{K} valley, whereas light with a polarization $\sigma = -$ couples the Landau levels -1 and $+0$ in the \mathbf{K}' valley. Furthermore, due to the spin-orbit gap, each transition is split into two rays $\Delta_B^{\xi s}$, such that one may furthermore identify each ray with a particular spin orientation of the involved electrons. This is depicted in Fig. 6. The frequency of the rays is thus a direct measure of the spin-orbit gap in MoS₂. Notice finally that, as calculated in Eqs. (26), the absorption peaks of light with polarization $\sigma = +$ (in the \mathbf{K} valley) are much stronger than those for $\sigma = -$ (in the \mathbf{K}' valley). This situation needs to be contrasted to the case of silicene, where due to a strong spin-orbit gap, the $n = 0$ Landau levels are both situated at the bottom of the conduction band (for a particular spin orientation) such that circularly polarized light excites electrons in both valleys, with roughly the same spectral weight.^{19,20}

2. Transitions in moderately doped MoS₂

The transitions discussed in the preceding paragraph are the only ones involving the $n = 0$ level and visible for undoped MoS₂, i.e., when the Fermi level is situated in the gap between the valence and the conduction band. In the case of moderate doping, that is, if the Fermi level ε_F is comprised between

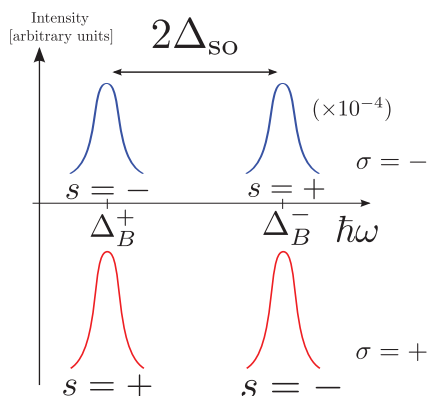


FIG. 6. (Color online) Schematic plot of light absorption as a function of energy. The color of the peaks indicates the corresponding polarization (red for $\sigma = +$ and blue for $\sigma = -$). Each peak corresponds to excitations for a single valley and value of the spin. The peaks are separated by $\Delta_{so} \approx 150$ meV. The peaks corresponding to $\sigma = -$ polarization are expected to be 10^4 smaller than the peaks corresponding to $\sigma = +$ polarization.

$\varepsilon_{-1}^{\xi s}$ and $\varepsilon_{+1}^{\xi s}$, other transitions involving $n = 1$ and 0 are possible. Indeed, using light of $\sigma = -$ polarization but of energy δ_B allows one to excite electrons in the valley \mathbf{K} , whereas a resonance at Δ_B is still associated with a transition from -1 to $+0$ in the \mathbf{K}' valley. In the case of a polarization $\sigma = +$, the role of the valleys is exchanged. Notice, however, that the resonances occur at extremely different energies since we have $\Delta_B^{\xi s} \approx 1.7$ eV, roughly independent of the magnetic field, whereas $\delta_B^{\xi s} \approx 0.27 B(T)$ meV is much smaller.

IV. DEVIATIONS FROM THE MAGNETO-OPTICAL SELECTION RULES DUE TO BAND CORRECTIONS

In contrast to the preceding section, where massive Dirac fermions were considered, the band structure of 2D MoS₂ reveals deviations from this ideal dispersion. The most prominent ones are the electron-hole asymmetry, which yields a mass difference of roughly 20% for electrons and holes,²³ and trigonal warping.¹⁰ In the present section, we investigate how these corrections affect the magneto-optical selection rules obtained above.

Similarly to monolayer graphene, trigonal warping arises from higher-order band corrections beyond linear order in the off-diagonal terms and may be accounted for via the term²⁴

$$\hat{H}_{3w} = \begin{pmatrix} 0 & \gamma(\xi q_x + i q_y)^2 \\ \gamma(\xi q_x - i q_y)^2 & 0 \end{pmatrix}, \quad (27)$$

whereas the electron-hole asymmetry is encoded in the corrective term

$$\hat{H}_{as} = \begin{pmatrix} \alpha q^2 & 0 \\ 0 & \beta q^2 \end{pmatrix}. \quad (28)$$

The relevant parameters may be obtained from a fit to tight-binding or *ab initio* calculations, and one finds $\alpha = 1.72$ eVÅ², $\beta = -0.13$ eVÅ², and $\gamma = -1.02$ eVÅ².¹⁰

A. Modified Landau levels

As in Sec. II C, the modified Landau-level spectrum may be obtained with the help of the Landau-Peierls substitution. The term \hat{H}_{as} remains diagonal in the basis of eigenstates of Eqs. (11)–(14) and reads

$$\hat{H}_{B,as}^{\xi,s} = \frac{1}{l_B^2} \begin{pmatrix} \alpha(2n+1) & 0 \\ 0 & \beta(2n+1) \end{pmatrix}. \quad (29)$$

Thus the eigenstates are of the same form as in Eqs. (11)–(14), with marginally different values of $\alpha_{\lambda n}^{\xi s}$. However, the energies levels are slightly shifted,

$$\varepsilon_{\lambda n}^{\xi s} = \frac{\alpha + \beta}{l_B^2} \left(n + \frac{1}{2} \right) + \lambda \sqrt{\left[\left(n + \frac{1}{2} \right) \frac{\alpha - \beta}{l_B^2} + \Delta_{\xi s} \right]^2 + n \varepsilon^2} \quad \text{for } \geq 1, \quad (30)$$

$$\varepsilon_{n=0}^{\xi s} = \frac{\alpha + \beta}{2l_B^2} - \xi \left(\frac{\alpha - \beta}{2l_B^2} + \Delta_{\xi s} \right). \quad (31)$$

In contrast to the electron-hole asymmetry term, the trigonal warping term^{24,25}

$$\hat{H}_{\mathbf{B},3w}^{\xi=+,s} = -\frac{2\gamma}{l_B^2} \begin{pmatrix} 0 & (a^\dagger)^2 \\ a^2 & 0 \end{pmatrix}, \quad (32)$$

$$\hat{H}_{\mathbf{B},3w}^{\xi=-,s} = -\frac{2\gamma}{l_B^2} \begin{pmatrix} 0 & a^2 \\ (a^\dagger)^2 & 0 \end{pmatrix} \quad (33)$$

is not diagonal in the basis (11)–(14) and thus needs to be treated perturbatively. Such a treatment shows that trigonal warping yields a second-order correction relative to the leading-order $(\hbar v_F/l_B)\sqrt{n}$ Landau-level behavior that arises only in second-order perturbation theory in γ .^{24,25} However, the eigenstates are modified at first order and one finds that the original eigenstate $\psi_{\lambda n}^{\xi,s}$ mixes with at most four states $\psi_{\lambda'n'}^{\xi,s}$ such that $n' = n \pm 3$. The modified eigenstate $\tilde{\psi}_{\lambda n}^{\xi,s}$ corresponding to the energy $\varepsilon_{\lambda n}^{\xi,s}$ is

$$\tilde{\psi}_{\lambda n}^{\xi,s} = \psi_{\lambda n}^{\xi,s} + \sum_{\substack{\lambda' = \pm \lambda \\ n' = n \pm 3}} \frac{(\psi_{\lambda'n'}^{\xi,s})^\dagger \hat{H}_{\mathbf{B},3w}^{\xi,s} \psi_{\lambda n}^{\xi,s}}{\varepsilon_{\lambda'n'}^{\xi,s} - \varepsilon_{\lambda n}^{\xi,s}} \psi_{\lambda'n'}^{\xi,s}. \quad (34)$$

Since $|\varepsilon_{-\lambda n'}^{\xi,s} - \varepsilon_{\lambda n}^{\xi,s}| \approx \Delta$ while $|\varepsilon_{\lambda n'}^{\xi,s} - \varepsilon_{\lambda n}^{\xi,s}| \approx \delta_B^{\xi,s} \ll \Delta$, the interband mixing with $\lambda' = -\lambda$ can be neglected in the sum. Evaluation of the matrix elements of $\hat{H}_{\mathbf{B},3w}^{\xi,s}$ yields

$$\tilde{\psi}_{\lambda n}^{\xi,s} \simeq \psi_{\lambda n}^{\xi,s} + \mu_{\lambda n}^{\xi,s} \psi_{\lambda(n-3)}^{\xi,s} + \nu_{\lambda n}^{\xi,s} \psi_{\lambda(n+3)}^{\xi,s} \quad (35)$$

with

$$\mu_{\lambda n}^{+,s} = \delta_{n \geq 3} \frac{\gamma (\beta_{n-3})^\dagger \alpha_{\lambda n}^{+,s} \sqrt{(n-1)(n-2)}}{l_B^2 N_{\lambda(n-3)}^{+,s} N_{\lambda n}^{+,s} (\varepsilon_{\lambda(n-3)}^{+,s} - \varepsilon_{\lambda n}^{+,s})}, \quad (36)$$

$$\mu_{\lambda n}^{-,s} = \delta_{n \geq 3} \frac{\gamma (\alpha_{\lambda(n-3)}^{-,s})^\dagger \beta_n \sqrt{(n-1)(n-2)}}{l_B^2 N_{\lambda(n-3)}^{-,s} N_{\lambda n}^{-,s} (\varepsilon_{\lambda(n-3)}^{-,s} - \varepsilon_{\lambda n}^{-,s})}, \quad (37)$$

$$\nu_{\lambda n}^{+,s} = \frac{\gamma (\alpha_{\lambda(n+3)}^{+,s})^\dagger \beta_n \sqrt{(n+2)(n+1)}}{l_B^2 N_{\lambda n}^{+,s} N_{\lambda(n+3)}^{+,s} (\varepsilon_{\lambda(n+3)}^{+,s} - \varepsilon_{\lambda n}^{+,s})}, \quad (38)$$

$$\nu_{\lambda n}^{-,s} = \frac{\gamma (\beta_{n+3})^\dagger \alpha_{\lambda n}^{-,s} \sqrt{(n+2)(n+1)}}{l_B^2 N_{\lambda n}^{-,s} N_{\lambda(n+3)}^{-,s} (\varepsilon_{\lambda(n+3)}^{-,s} - \varepsilon_{\lambda n}^{-,s})}, \quad (39)$$

where $\delta_{n \geq 3}$ symbolically indicates that $\mu_{\lambda n}^{\xi,s}$ is nonzero only for $n \geq 3$. For these expressions to remain valid for the zero states, one may define $\psi_{\lambda n}^{\xi=-\lambda,s} = 0$ and $\alpha_{\lambda 0}^{\xi,s} = \beta_0 = 1$. Considering that $\gamma/l_B^2 \ll \alpha_{\xi s}^{\lambda n}$ or β_n , it is a good approximation to say that the norm $N_{\lambda n}^{\xi,s}$ is unchanged for small values of n .

B. Optical transitions

With the help of the above-mentioned states, it is possible to examine the effect of the additional terms on the optical transitions. To that effect, one may use the same formalism as in Sec. III A. To take into account the addition of \hat{H}_{as} and \hat{H}_{3w} , one has to change the $\hat{W}_{\xi\sigma}$ matrix of Eq. (21) into

$\hat{W}_{\xi\sigma}^{\text{tot}} = \hat{W}_{\xi\sigma} + \hat{W}_{\xi\sigma}^1$ with

$$\hat{W}_{+\xi}^1 = \frac{Ae}{l_B \hbar} \begin{pmatrix} \alpha i \sqrt{2} a^\dagger & -i \sqrt{2} \gamma (1 - \xi) a \\ i \sqrt{2} \gamma (1 + \xi) a^\dagger & \beta i \sqrt{2} a^\dagger \end{pmatrix}, \quad (40)$$

$$\hat{W}_{-\xi}^1 = \frac{Ae}{l_B \hbar} \begin{pmatrix} -\alpha i \sqrt{2} a & i \sqrt{2} \gamma (1 + \xi) a^\dagger \\ -i \sqrt{2} \gamma (1 - \xi) a & -\beta i \sqrt{2} a \end{pmatrix}.$$

Two types of corrections, to first order in γ (and principally also in α and β), need to be considered. First, the perturbed states (35) allow for additional transitions when evaluated in the unperturbed coupling Hamiltonian (20), due to the mixing between $\tilde{\psi}_{\lambda n}^{\xi,s}$ and $\psi_{\lambda(n \pm 3)}^{\xi,s}$. In this case, the previous selection rules apply, and thus $n' = n \pm 3 \pm 1$, i.e., $n' = n \pm 2$ or $n' = n \pm 4$. Second, the modified light-matter coupling $\hat{W}_{\xi\sigma}^1$ yields additional transitions when evaluated in the unperturbed states, such as, for example, the interband transition $n \rightarrow n$. These transitions arise from the nondiagonal terms in Eq. (40), whereas the diagonal terms yield dipolar transitions $n \rightarrow n \pm 1$, such as the ones discussed in Sec. III. Table I can be used to determine the relative magnitude of the transitions. The value for the $\tilde{\psi}_{\lambda n}^{\xi,s} \rightarrow \tilde{\psi}_{\lambda'n'}^{\xi,s}$ transition relative amplitude with $n' = n \pm 2$ or 4 is the amplitude for $\psi_{\lambda(n \pm 3)}^{\xi,s} \rightarrow \psi_{\lambda'n'}^{\xi,s}$ normalized with the adequate factor, either $|\mu_{\lambda n}^{\xi,s}/N_{\lambda n}^{\xi,s}|^2$ or $|\nu_{\lambda n}^{\xi,s}/N_{\lambda n}^{\xi,s}|^2$. Other possible transitions involving both the perturbed states and the corresponding light matrix elements are proportional to at most $l_B^{-4} \propto B^2$ and can thus be neglected to first order in perturbation theory.

Henceforth, trigonal warping and electron-hole asymmetry induce additional transitions $\psi_{\lambda n}^{\xi,s} \rightarrow \psi_{\lambda'n'}^{\xi,s}$ with $n' = n$, $n' = n \pm 2$, or $n' = n \pm 4$. One may want to evaluate the relative intensity of corresponding absorption peaks, at least for small values of n . For transitions involving the $\hat{W}_{\xi\sigma}$ light matrix and perturbed $\tilde{\psi}_{\lambda n}^{\xi,s}$ states, the evaluation of $|\mu_{\lambda n}^{\xi,s}/N_{\lambda n}^{\xi,s}|^2$ shows that, for $B = 10$ T, the $n' = n \pm 3 \pm 1$ peaks should be about 3000 times smaller than the regular peaks corresponding to $\psi_{\lambda(n \pm 3)}^{\xi,s} \rightarrow \psi_{\lambda'n'}^{\xi,s}$ transitions. Similarly, the $n' = n$ peaks originating from the additional terms in the light coupling can be evaluated to be about 1000 times smaller than the regular peaks.

V. CONCLUSIONS

In summary, we have used a two-band model that reduces to massive Dirac fermions with a spin-valley-dependent gap at low energies to investigate the magneto-optical properties of MoS₂. Most saliently, the particular behavior of the $n = 0$ Landau levels, which stick to the top of the valence band and the bottom of the conduction band in the \mathbf{K} and \mathbf{K}' valleys, respectively, allows for a selection of electrons in a particular valley via the circular polarization of the light field. Whereas the $-0 \rightarrow +1$ transition (in the valley \mathbf{K}) is addressed by the polarization $\sigma = +$, the $-1 \rightarrow +0$ transition (in the valley \mathbf{K}') couples only to light with a polarization $\sigma = -$. Moreover, because of the moderate spin-orbit gap (mainly in the valence band), it is possible to address electrons with a particular spin orientation. Indeed, a resonant excitation of the above-mentioned Landau level transitions would allow not only to excite electrons in a single valley (via the circular

polarization of the light) but also a single spin state in that valley because the resonance condition is spin-dependent. In light transmission measurements of MoS₂ flakes in a magnetic field, for example, one would therefore expect two absorption peaks for each polarization separated by the spin-orbit gap. This would allow for a direct spectroscopic measurement of the spin-orbit coupling in MoS₂ in the vicinity of the **K** points.

The analysis remains valid for other systems sharing the low-energy structure of MoS₂, as might be the case for other group-VI dichalcogenides.¹² Beyond the description of low-energy electrons in MoS₂ in terms of massive Dirac fermions, which yields the typical dipole-type magneto-optical selection rules $n \rightarrow n \pm 1$ (regardless of the bands involved),

we have shown that higher-order band corrections give rise to nondipolar magneto-optical transitions. Whereas to first order in perturbation theory the Landau-level spectrum is affected only by the particle-hole asymmetry, but not by trigonal warping, the latter induces additional transitions already at first order. As such, we have identified the interband transition $n \rightarrow n$ as well as $n \rightarrow n \pm 2$ and $n \rightarrow n \pm 4$. These transitions are expected to cause additional absorption peaks in light transmission experiments, albeit with a significantly lower spectral weight as compared to the dipolar transitions.

ACKNOWLEDGMENT

We acknowledge fruitful discussions with Marek Potemski.

-
- ¹K. S. Novoselov, D. Jiang, F. Schedin, T. J. Booth, V. V. Khotkevich, S. V. Morozov, and A. K. Geim, *Proc. Natl. Acad. Sci. USA* **102**, 10451 (2005).
- ²K. F. Mak, C. Lee, J. Hone, J. Shan, and T. F. Heinz, *Phys. Rev. Lett.* **105**, 136805 (2010).
- ³A. Splendiani, L. Sun, Y. Zhang, T. Li, J. Kim, C.-Y. Chim, G. Galli, and F. Wang, *Nano Lett.* **10**, 1271 (2010).
- ⁴H. Rostami, A. G. Moghaddam, and R. Asgari, *Phys. Rev. B* **88**, 085440 (2013).
- ⁵E. Cappelluti, R. Roldán, J. A. Silva-Guillén, P. Ordejón, and F. Guinea, *Phys. Rev. B* **88**, 075409 (2013).
- ⁶H. Ochoa and R. Roldan, *Phys. Rev. B* **87**, 245421 (2013).
- ⁷L. F. Mattheiss, *Phys. Rev. B* **8**, 3719 (1973).
- ⁸S. Lebègue and O. Eriksson, *Phys. Rev. B* **79**, 115409 (2009).
- ⁹T. Cheiwchanchamnangij and W. R. L. Lambrecht, *Phys. Rev. B* **85**, 205302 (2012).
- ¹⁰A. Kormányos, V. Zólyomi, N. D. Drummond, P. Rakyta, G. Burkard, and V. I. Fal'ko, *Phys. Rev. B* **88**, 045416 (2013).
- ¹¹W. S. Yun, S. W. Han, S. C. Hong, I. G. Kim, and J. D. Lee, *Phys. Rev. B* **85**, 033305 (2012).
- ¹²D. Xiao, G.-B. Liu, W. Feng, X. Xu, and W. Yao, *Phys. Rev. Lett.* **108**, 196802 (2012).
- ¹³A. H. Castro-Neto, F. Guinea, N. M. R. Peres, K. S. Novoselov, and A. K. Geim, *Rev. Mod. Phys.* **81**, 109 (2009).
- ¹⁴H. Zeng, J. Dai, W. Yao, D. Xiao, and X. Cui, *Nat. Nanotech.* **7**, 490 (2012).
- ¹⁵K. F. Mak, K. He, J. Shan, and T. F. Heinz, *Nat. Nanotech.* **7**, 494 (2012).
- ¹⁶T. Cao, J. Feng, J. Shi, Q. Niu, and E. Wang, *Nat. Commun.* **3**, 887 (2012).
- ¹⁷D. Xiao, W. Yao, and Q. Niu, *Phys. Rev. Lett.* **99**, 236809 (2007).
- ¹⁸J.-N. Fuchs, F. Piéchon, M. O. Goerbig, and G. Montambaux, *Eur. Phys. J. B* **77**, 351 (2010).
- ¹⁹C. J. Tabert and E. J. Nicol, *Phys. Rev. Lett.* **110**, 197402 (2013).
- ²⁰C. J. Tabert and E. J. Nicol, *Phys. Rev. B* **88**, 085434 (2013).
- ²¹C. L. Kane and E. J. Mele, *Phys. Rev. Lett.* **95**, 226801 (2005).
- ²²M. Ezawa, *Phys. Rev. Lett.* **109**, 055502 (2012).
- ²³F. Zahid, L. Liu, Y. Zhu, J. Wang, and H. Guo, arXiv:1304.0074.
- ²⁴For a review, see M. O. Goerbig, *Rev. Mod. Phys.* **83**, 1193 (2011).
- ²⁵P. Plochocka, C. Faugeras, M. Orlita, M. L. Sadowski, G. Martinez, M. Potemski, M. O. Goerbig, J.-N. Fuchs, C. Berger, and W. A. de Heer, *Phys. Rev. Lett.* **100**, 087401 (2008).